Available online at www.sciencedirect.com

ScienceDirect

Ceramics International 40 (2014) 1747–1757

CERAMICS INTERNATIONAL

www.elsevier.com/locate/ceramint

Sol–gel synthesis of nanostructured titania–silica mesoporous membranes with photo-degradation and physical separation capacities for water purification

Vahideh Tajer-Kajinebaf[a], Hossein Sarpoolaky[a,*], Toraj Mohammadi[b]

[a]School of Metallurgy and Materials Engineering, Iran University of Science & Technology, Tehran, Iran
[b]Research Laboratory for Separation Processes, Faculty of Chemical Engineering, Iran University of Science and Technology, Tehran, Iran

Received 19 May 2013; received in revised form 6 July 2013; accepted 15 July 2013
Available online 22 July 2013

Abstract

The effect of silica addition on the photocatalytic and separation properties of mesoporous titania–silica membranes was investigated. Macroporous α-alumina support was used as substrate, and intermediate layer was obtained by deposition and calcination of the colloidal titania sol on the substrate. Then, titania and titania-5% silica polymeric sols were prepared for deposition on the interlayer as membrane top layer. The samples were characterized by DLS, TG-DTA, XRD, FTIR, BET, FESEM, TEM and AFM. The photocatalytic capability of the membranes was evaluated using methyl orange photo-degradation. The mesoporous composite membrane was prepared with the average pore size of 3.94 nm. The dye removal efficiency of the titania–silica membrane has been determined to be 63% after 60 min UV-irradiation. By coupling separation process with photocatalytic technique, the removal efficiency was improved up to 94%. The synthesized titania–silica membrane showed a great potential due to its multifunctional capability for water treatment.

Keywords: A. Sol–gel; B. Composite; E. Membrane; TiO_2–SiO_2

1. Introduction

Nowadays water pollution, caused by hazardous organic materials, is a very serious problem [1]. Ceramic membranes can play a very important role in separation technology for water purification [2]. Membrane separation techniques have already shown to be competitive with other separation techniques for what concerns material recovery and achievement of processes with selective removal of some components [3]. However, this method only transfers pollutants from a phase to another and displays a simple separation role [4]. On the other hand, photocatalytic process is introduced as a promising technology for the water purification [5,6]. Photocatalysts have also been widely used for the decomposition of harmful compounds in environment and photocatalytic reactions allow in many cases a complete degradation of organic pollutants, without using chemical materials [7,8]. The coupling of photocatalytic process with membrane separation technique can take advantage of the synergy of both technologies resulting in a powerful system, with the membrane having the simultaneous task of supporting the photocatalyst as well as acting as a selective barrier for the species to be degraded [4,9–11]. Among different materials utilized for membrane and photocatalytic applications, titania is the most attractive materials due to its unique properties like high photocatalytic activity, high chemical stability, high liquid flux [12], and inexpensive price [1]. Thus, titania membranes are being used for different applications such as water treatment [2,9,11,13]. Although titania has been known as the most effective material in photocatalytic processes, the relatively low surface area and the instability of the titania anatase phase at high temperatures are disadvantages [14]. As photocatalytic activity of titania is greatly influenced by its crystal structure, surface area, crystallite size, surface hydroxyl content, porosity [15,16], and incident light intensity but the

*Corresponding author. Tel.: +98 21 77240540x550; fax: +98 21 77240480.
E-mail addresses: vtajer@yahoo.com (V. Tajer-Kajinebaf), hsarpoolaky@iust.ac.ir (H. Sarpoolaky), torajmohammadi@iust.ac.ir (T. Mohammadi).

0272-8842/$ - see front matter © 2013 Elsevier Ltd and Techna Group S.r.l. All rights reserved.
http://dx.doi.org/10.1016/j.ceramint.2013.07.074

crystal structure and surface area can be considered as the most important factors for determining the photoactivity. Many researchers reported that anatase is the most photoactive polymorph of titania [17,18], although it is thermodynamically metastable [19]. To obtain highly active titania photocatalyst, it is necessary to develop temperature stability of anatase phase along with increasing the surface area. Therefore, many efforts have been devoted to inhibit crystal growth and retarding phase transformation by incorporating another inorganic oxide into the titania frameworks [1,18,20,21]. It has been reported that silica addition has a significant influence on the surface properties [16] and enhancement of titania photoactivity [22–24]. Anderson and Bard [23,25] demonstrated that a mixed oxide of titania and silica is a more efficient photocatalyst for the photo-degradation of some compounds than pure titania [26,27]. The mixed oxides of titania and silica seem to be a good alternative to retard anatase-rutile phase transformation as well as to stabilize porosity structure at high temperatures.

On the basis of our knowledge, there are limited researches on the sol–gel synthesis of the nanostructured titania–silica mesoporous membranes with photocatalytic and physical separation capabilities for water purification. In the present work, the nanostructured titania and titania–silica mesoporous membranes were prepared via the polymeric sol–gel route on the colloidal titania-coated alumina substrate, and were characterized by DTA-TG, XRD, FTIR, BET, FESEM, TEM and AFM. Then, the effect of silica addition was investigated on the properties of the titania-silica composite membrane. Finally, the photocatalytic and separation capabilities of the prepared membranes were evaluated by calculation of the methyl orange removal efficiency in aqueous solution.

2. Experimental procedures

2.1. Materials

Alumina disk supports were used as the membrane substrate with the properties shown in Table 1.

Titanium tetraisopropoxide ($Ti(Opri)_4$, Merck 821895), tetraethyl orthosilicate ($Si(OEt)_4$, Merck 800658), isopropanol (IPA, Merck 109634), ethanol (EtOH, Merck 100983), hydrochloric acid (37% solution, Merck, 100317) and deionized water were used as raw materials for the preparation of titania and silica sols. Methyl orange (MO, Merck 101322) with chemical formula of $C_{14}H_{14}N_3NaO_3S$ was used as the model pollutant for the investigation of photocatalytic and separation capabilities of the titania and titania–silica membranes.

2.2. Membrane preparation

The membrane intermediate layer was prepared by deposition and calcination of colloidal titania sol on the alumina support. In our previous research, the preparation method of the colloidal titania-coated alumina substrates have been thoroughly explained [9]. Membrane top layer was prepared by deposition and calcination of pure titania and titania-5% silica polymeric sols on the intermediate layer. For this purpose, titania polymeric sol was obtained by hydrolysis of $Ti(Opri)_4$ via the addition of a less than equivalent amount of H_2O ($[H_2O]/[Ti] < 4$) in order to obtain a precipitate free polymeric sol. A solution of water and hydrochloric acid as a catalyst in IPA was added dropwise to a solution of $Ti(Opri)_4$ in IPA during high speed stirring. The molar ratio for $Ti(Opri)_4$: IPA: H_2O: HCl of the final sol was 1: 31: 0.8: 0.23, respectively. Stirring was continued for 4 h to get a stabilized sol. The obtained product was a transparent titania polymeric sol. Also, a precipitate free silica polymeric sol was obtained similar to titania polymeric sol by hydrolysis of $Si(OEt)_4$ with molar ratio of $Si(OEt)_4$: EtOH: H_2O: HCl = 1: 20.1: 1: 0.2. Then, a stable titania–silica composite sol was prepared by physical mixing of the synthesized titania and silica polymeric sols in a mole ratio of 5% silica. After stirring for 3 h, the titania and titania–silica polymeric sols were deposited on the colloidal titania-coated alumina substrate by dip-coating process with a constant rate of 6 mm/min and immersion time of 30 s. Also, the unsupported gel layers were prepared by pouring the polymeric sols in a petri-dish. The supported and unsupported gel layers were dried at room temperature for 24 h. Then, heat-treatment was done at different temperatures for 1 h with a heating rate of 1 °C/min. Finally, the supported and unsupported membranes were obtained. Fig. 1 presents the preparation steps of the titania–silica composite membrane.

In this paper, the pure titania and titania-5% silica are denoted as PT and TS, respectively. This research focuses on the characterization of the PT and TS membranes synthesized by polymeric sol–gel route and investigates the effect of silica addition on the properties of the supported and unsupported composite membranes.

2.3. Characterization

The properties of the synthesized samples are investigated using individual parts containing unsupported and supported membranes.

2.3.1. Unsupported membranes

Particle size distribution of the prepared PT and TS polymeric sols was determined by dynamic light scattering technique (DLS,

Table 1
Properties of the membrane substrate.

Composition	Disk size (mm)	Strength (MPa)	Pore size (μm)	Water absorption (%)	Open porosity (%)
α-Alumina (KMS-92, Martinswerk)	Dia. = 17, Thick. = 2	38	1–3	14–17	39–42

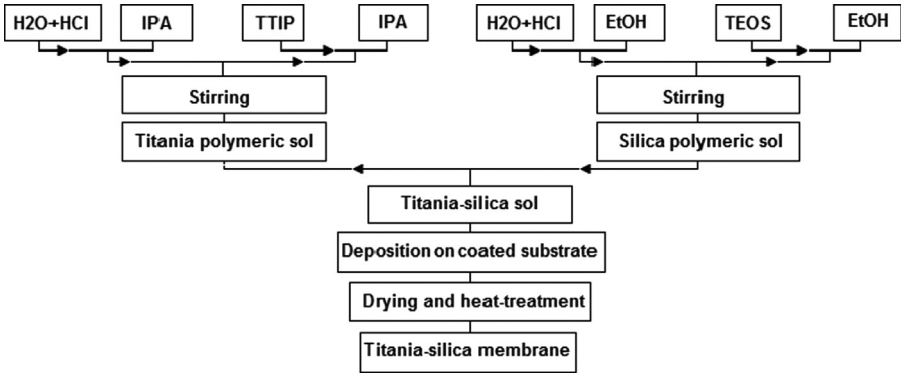

Fig. 1. Preparation steps of the titania–silica composite membrane.

ZS3600, Malvern). Thermal properties of the dried gels were characterized by thermogravimetry and differential thermal analysis (TG-DTA, PERKINELMER) in a nitrogen flow with a heating rate of 7.5 °C/min up to 900 °C. The phase composition and the average crystallite size were identified using X-ray diffraction technique with Cu Kα wavelength at 30 mA and 40 kV (XRD, Philips PW1800). Fourier transform infrared spectroscopy (FTIR, 8400 S, Shimadzu) was performed to investigate structural and specific molecule-groups information on wafers consisting of 100 mg dry KBr and about 1 mg sample. N_2 adsorption and desorption measurements were performed (Belsorp mini II, BEL Japan, Inc.) to determine the Brunauer–Emmett–Teller (BET) surface area and the pore size of samples.

2.3.2. Supported membrane

The morphology of the membranes was characterized by field emission scanning electron microscopy (FESEM, WEGA\ \TESCAN) and transmission electron microscopy (TEM, EM 208, Philips) with an accelerating voltage of 30–100 kV, respectively. Surface morphology and topography of the prepared membranes was evaluated by atomic force microscopy (AFM, DualScope C-26, DME). Also, the photocatalytic activity of the membranes was measured by the photodegradation of MO aqueous solution. Initial pollutant concentration was set at 20 mg/l and membranes in this solution were irradiated by a UV source (Sunny, 360–415 nm, 125 W). The MO removal efficiency was estimated by applying the following Eq. (1):

$$\text{Removal efficiency}(\%) = [(C_0 - C)/C_0] \times 100, \quad (1)$$

where C_0 is the original MO concentration and C is the residual MO concentration in the feed solution [27].

The dye separation performance of aqueous solution was investigated using a photocatalytic membrane setup with a dead-end filtration cell under 5 bar pressure according to Fig. 2.

Also, water permeability was determined using the as-prepared membrane setup. The feed side of the membrane was kept at a constant pressure of 5 bar and the permeate side was set at atmospheric pressure. The permeation flux was measured at room temperature using the following Eq. (2) [28]:

$$\text{Permeation flux} = V/A\Delta t, \quad (2)$$

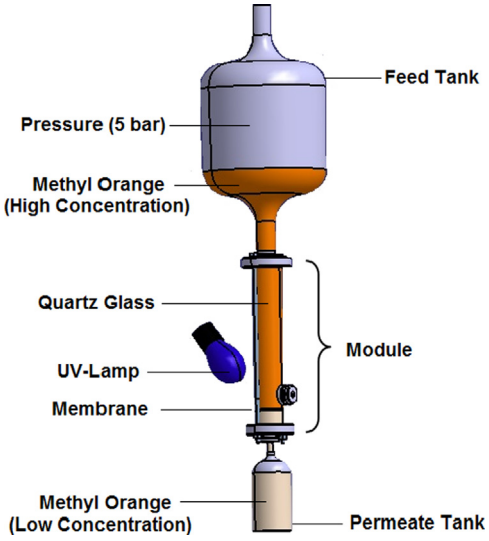

Fig. 2. Schematic image of a photocatalytic membrane setup with a dead-end filtration cell used for filtration experiments.

where V is the quantity of permeate (L), A is the effective membrane area (m^2) and Δt is the sampling time (h). Effective area of the membrane in the module was 1.76 cm^2. Permeation experiment is recommended as one of the most important methods to find the structure and morphology of prepared membranes [29].

3. Results and discussion

3.1. Unsupported membranes

3.1.1. Particle size distribution

Particle size distribution of the prepared PT and TS polymeric sols is shown in Fig. 3.

The particle size distribution of the TS sol is determined to be in the range of 0.3–1.1 nm with the average particle size of 0.55 nm. As seen, the particle size distribution of the TS composite sol is narrower than that of the PT sol which can be attributed to the decrease in titanium percentage. This may be interpreted on the basis of the fact that titanium is a transition metal with electropositive charge. Values of δ(M) calculated from the partial charge model δ(M) of $Ti(OEt)_4$ and $Si(OEt)_4$ are +0.63

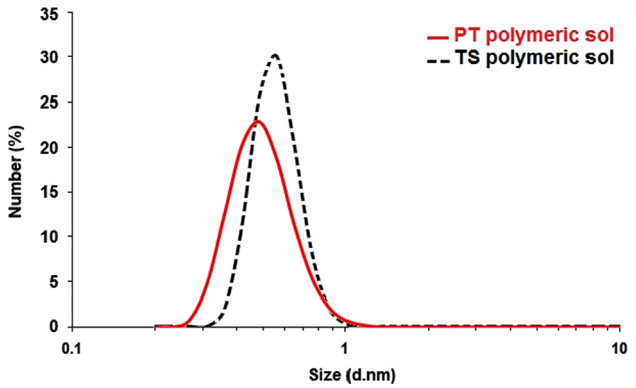

Fig. 3. Particle size distribution of the PT and TS polymeric sols.

and +0.32, respectively. Thus, titanium has duplex silicon of electropositive charge which explains why the hydrolysis and condensation kinetics of $Ti(Opri)_4$ are much faster than those of $Si(OEt)_4$. In this regard, hydrolysis rate of $Ti(Opri)_4$ is more 10–100 times than $Si(OEt)_4$ [27]. Thus, the rapid hydrolysis of $Ti(Opri)_4$ causes smaller particles with a wider distribution. It seems that $Si(OEt)_4$ addition to titania sol decreases the particle size distribution due to control hydrolysis rate.

3.1.2. Thermal analysis properties

TG and DTA curves of the dried PT and TS polymeric gels are presented in Fig. 4. The thermograms of both samples show a rather similar behavior.

According to Fig. 4a, TG curves follow a three-step weight loss consisting of alcohol and adsorbed water evaporation, alkoxide groups removal and $Ti(OH)_4$ dehydroxylation, respectively. The weight loss due to dehydroxylation is detected between 370 and 420 °C for the dried PT gel which is seen at higher temperatures in the case of the TS composite. It seems that silica addition influences on the gel structure and changes decomposition behavior.

DTA curves of the PT and TS gels are presented in Fig. 4b. Desorption of physically bonded water and organic solvents from the gel takes place at around 80 °C for both samples. For the PT sample, exothermic peaks are seen at 300, 360 and 410 °C which are related to dehydroxylation of $Ti(OH)_4$, removal of alkoxide groups and titania crystallization, respectively. These peaks are shifted to higher temperatures in the case of TS composite due to silica addition [30]. The weight loss ends at about 500 °C so it can be chosen as the lowest calcination temperature in which the removal of organic materials is completed.

3.1.3. Phase analysis

Fig. 5 presents XRD patterns of the PT and TS samples calcined at different temperatures.

Significant peak of anatase phase for both samples is observed at 400 °C and its intensity increases at higher temperatures. For the PT sample, rutile peaks are clearly seen at 800 °C while no peaks of rutile and brookite are detected for the TS composite at this temperature. It is confirmed that the TS composite has higher thermal stability and suppresses the

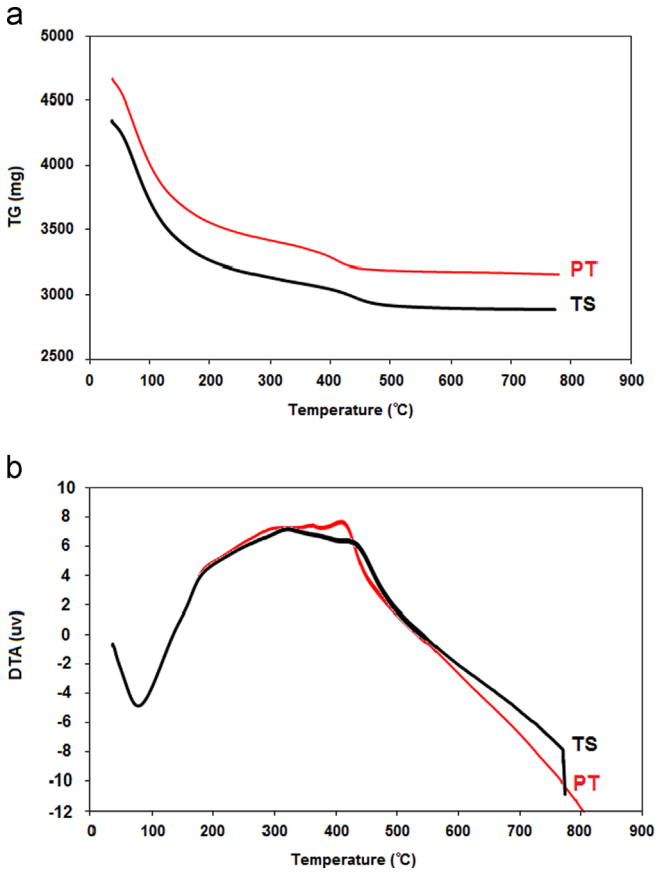

Fig. 4. (a) TG and (b) DTA curves of the dried PT and TS polymeric gels.

phase transformation from anatase to rutile. It seems that silica prevents the nucleation of rutile by impeding the mutual contact of titania crystals. This is proposed as the reason for the observed retarding effect on the anatase-rutile transformation. It has been reported that solid solution formation of anatase and silica may be responsible for the observed inhibiting effect on the phase transformation [22]. For investigation of the inhibiting effect of silica on anatase-rutile phase transformation, the lattice parameters of anatase were measured by X'Pert HighScore Plus software. Table 2 compares the lattice parameters, theoretical density and unit cell volume of anatase structure for the PT and TS samples calcined at 500 °C.

On the basis of results, the TS composite shows about 0.27% reduction in volume of unit cell compared to the PT sample. It clearly suggests the formation of an anatase solid solution containing silica since the ionic radium of Si^{4+} (0.042 nm) is smaller than that of Ti^{4+} (0.068 nm) [31].

For PT and TS samples, the anatase crystallite size was determined by Scherrer's equation [32] as recorded in Table 3.

On the basis of these results, the crystallite size increases with increasing calcination temperature while the growth rate is slower for the TS composite. The results confirm that the embedding of silica into titania inhibits the growth of anatase titania crystal as claimed by Zhang et al. [33]. Periyat et al.

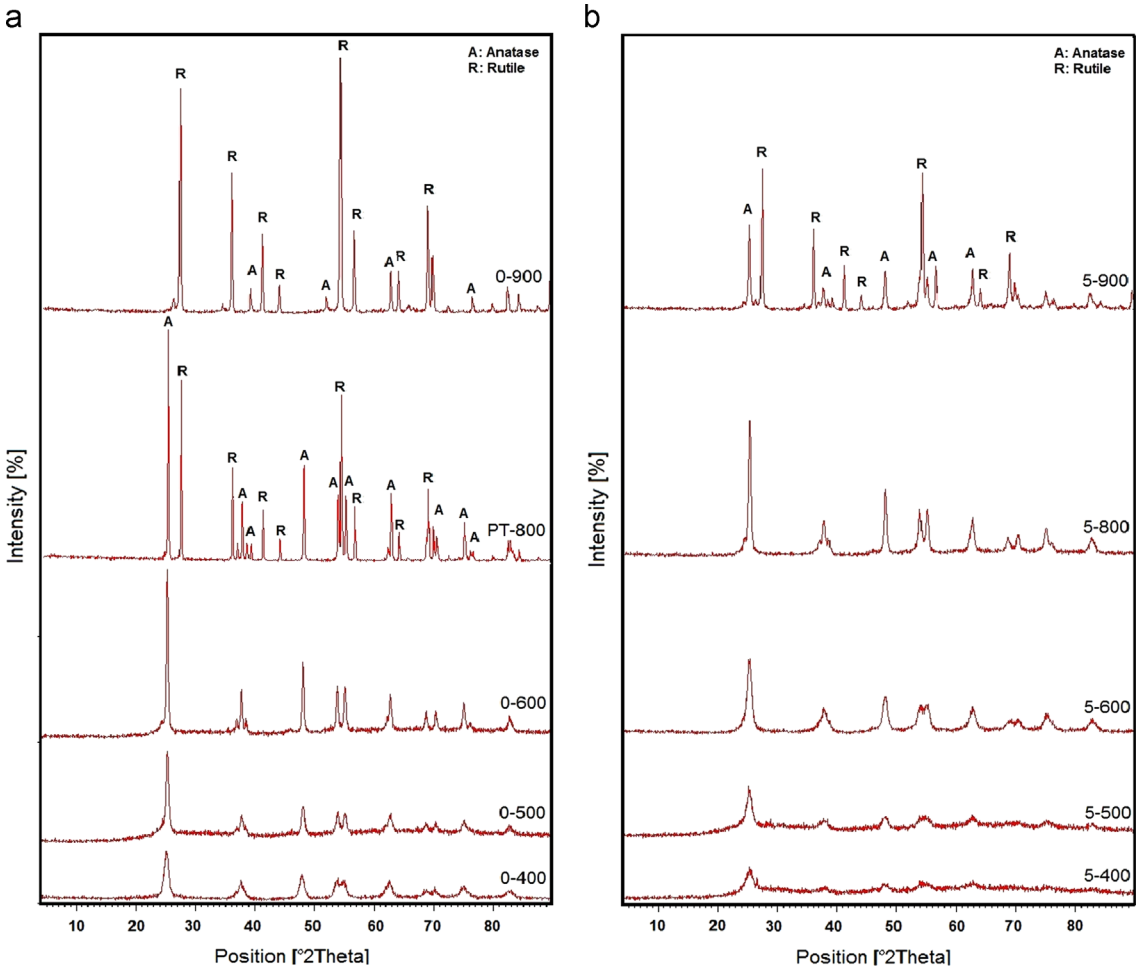

Fig. 5. XRD patterns of the (a) PT and (b) TS samples calcined at different temperatures.

Table 2
Unit cell properties of anatase structure for the PT and TS samples calcined at 500 °C.[a]

	Lattice parameters (nm)			Theoretical density (g/cm^3)	Volume of cell (nm^3)	Structure
	a	*b*	*c*			
PT	3.7852	3.7852	9.5139	3.89	136.31	Tetragonal
TS	3.7822	3.7822	9.5023	3.90	135.93	Tetragonal

[a]calculated by new x'pert software.

Table 3
Anatase crystallite size for the PT and TS samples.

Temperature (°C)	Anatase crystallite size (nm)	
	PT	TS
400	9.4	8.6
500	23.8	9.6
600	29.5	16.9
800	51.9	23
900	–	32

reported that the movement of Si^{4+} ions into the titania matrix leads to the reduction in anatase/anatase contact points which may reduce the growth of anatase crystals [31]. Also, Sibu et al. stated that silica addition results in the reduction of crystallite size due to the distribution of doped cations on the surface of titania. Therefore, such smaller crystals inhibit grain growth by providing a barrier between titania grains [34].

It is reported that the highest photocatalytic activity of titania is seen in the anatase form with optimal crystallite size in the range of 8–10 nm [35]. However, XRD results show that the PT and TS samples calcined at 500 °C are in the fully anatase crystalline form with a crystallite size less than 10 nm. Thus, based on TG-DTA and XRD results, 500 °C temperature was selected as an optimum temperature for calcination of the membrane top layer. It should be noted that the low calcination temperature makes it possible to prepare membranes with the reduced pore and crystallite sizes [36].

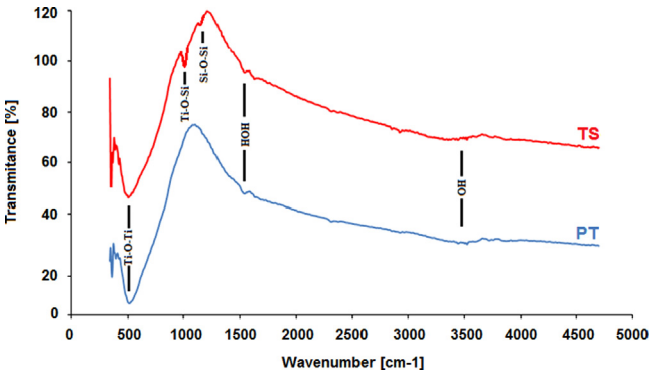

Fig. 6. FTIR spectra of the PT and TS samples.

3.1.4. FTIR analysis

Chemical structure of the PT and TS samples was studied by FTIR analysis. Fig. 6 presents the FTIR spectra of both samples in the wave number range from 4700 to 400 cm^{-1}.

In both spectra, the FTIR peaks around 3400 and 1622 cm^{-1} are attributed to stretching mode of water and hydroxyl [37–39]. TiO_2 retains adsorbed water due to the strong Lewis acidity of the unsaturated Ti^{4+} surface sites. Ti–O–Ti vibration appears in the range of 400–600 cm^{-1} as the result of condensation reaction. Also, the peaks at 1087 or 1110 cm^{-1} correspond to the asymmetric stretching vibration of Si–O–Si. Theoretically, two types of interaction between TiO_2 and SiO_2 are possible: physically mixed due to weak Van der Waals forces and chemically bonded due to formation of Ti–O–Si linkages [32]. The IR band observed at 910–960 cm^{-1} might be due to the stretching vibration band of Ti–O–Si bonds [18,24,39,40]. As a result, the IR band observed at 930 cm^{-1} in the spectra of the TS composite indicates the possibility of formation of Ti–O–Si bonds. According to the FTIR results, the formation of Si–O–Ti cross-linking bonds and –OH radicals around the Ti–O network can restrict the growth of grains during heat treatment.

3.1.5. N_2 adsorption and desorption studies

N_2 adsorption and desorption isotherms as well as BJH pore size distribution of the PT and TS samples are shown in Fig. 7.

According to Fig. 7a, both samples show nearly similar adsorption patterns. The nature of adsorption isotherms displays a type IV adsorption isotherm with a hysteresis loop classified as type H_2 according to IUPAC [41]. Isotherms indicate that a major fraction of the pores is in the mesopore range. There is an increase in the adsorption in all the relative pressure regions for the TS composite compared to the PT sample. Thus, it seems that the addition of 5% silica has increased total pore volume in the composite sample.

According to Fig. 7b, the pore distribution of the PT sample is in the range of 1–9 nm with an average radius at around 3.55 nm as calculated by the BJH method from both adsorption and desorption curves. For the TS composite, the pore distribution is very narrow in the range of 1–4 nm with an average radius at around 1.88 nm. In other words, the pore size of the titania sample sharply decreases with silica addition.

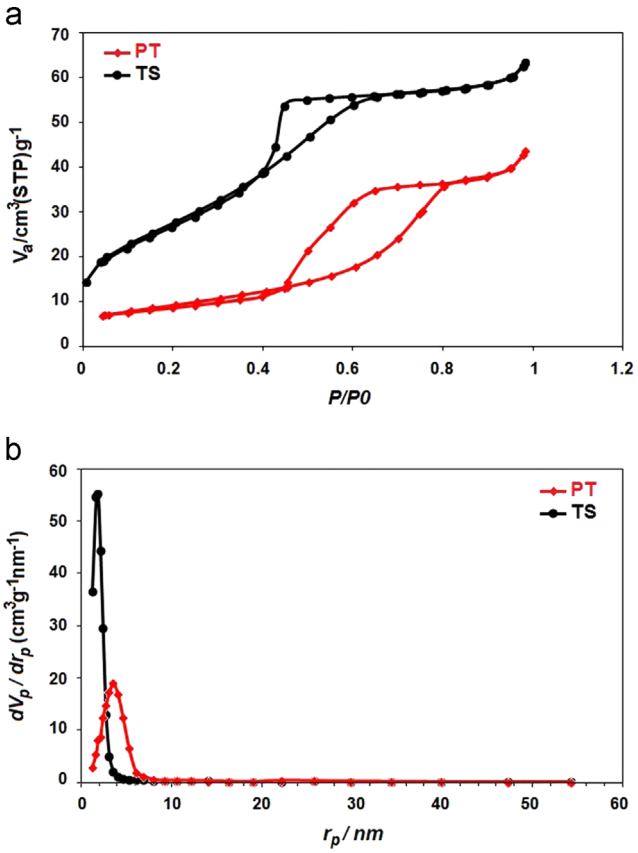

Fig. 7. The results obtained by BET analysis for the PT and TS samples: (a) N_2 adsorption and desorption isotherms and (b) BJH pore size distribution.

The structural characteristics of the PT and TS samples are summarized in Table 4.

Based on these results, with addition of 5% silica, the surface area increases from 32.8 m^2/g up to 99.14 m^2/g. Also, the total pore volume increases up to 0.097 cm^3/g as derived from the amount of N_2 adsorbed at p/p_0 of 0.99.

3.2. Supported membranes

3.2.1. Microstructural studies

3.2.1.1. FESEM. FESEM images of the surface and the cross-section of the PT and TS membranes are shown in Fig. 8.

According to Fig. 8a and c, both membranes show an approximately uniform surface with a granular morphology. Comparing Fig. 8b and d, shows the thickness of the TS membrane is a little more than that of the PT membrane in the same preparation conditions.

3.2.1.2. TEM. TEM micrographs of the PT and TS membranes are shown in Fig. 9.

As revealed by TEM micrographs, both membranes consist of large particles that are agglomerations of smaller particles in nanometer scale. It can be seen that the grain size of the TS membrane is clearly smaller than that of the PT membrane. The grain size of the TS composite membrane is estimated at

Table 4
Structural characteristics of the PT and TS samples.

	S_{BET} (m^2/g)[a]	V_p (cm^3/g)[b]	D_{BJH} (nm)[c]	$r_{p,peak}$ (nm)[d]
PT	32.80	0.067	8.17	3.55
TS	99.14	0.097	3.94	1.88

[a]Specific surface area.
[b]Total pore volume.
[c]Pore diameter determined from the adsorption branch using the Barret–Joyner–Halende (BJH) model.
[d]Pore radius in peak of BJH curve.

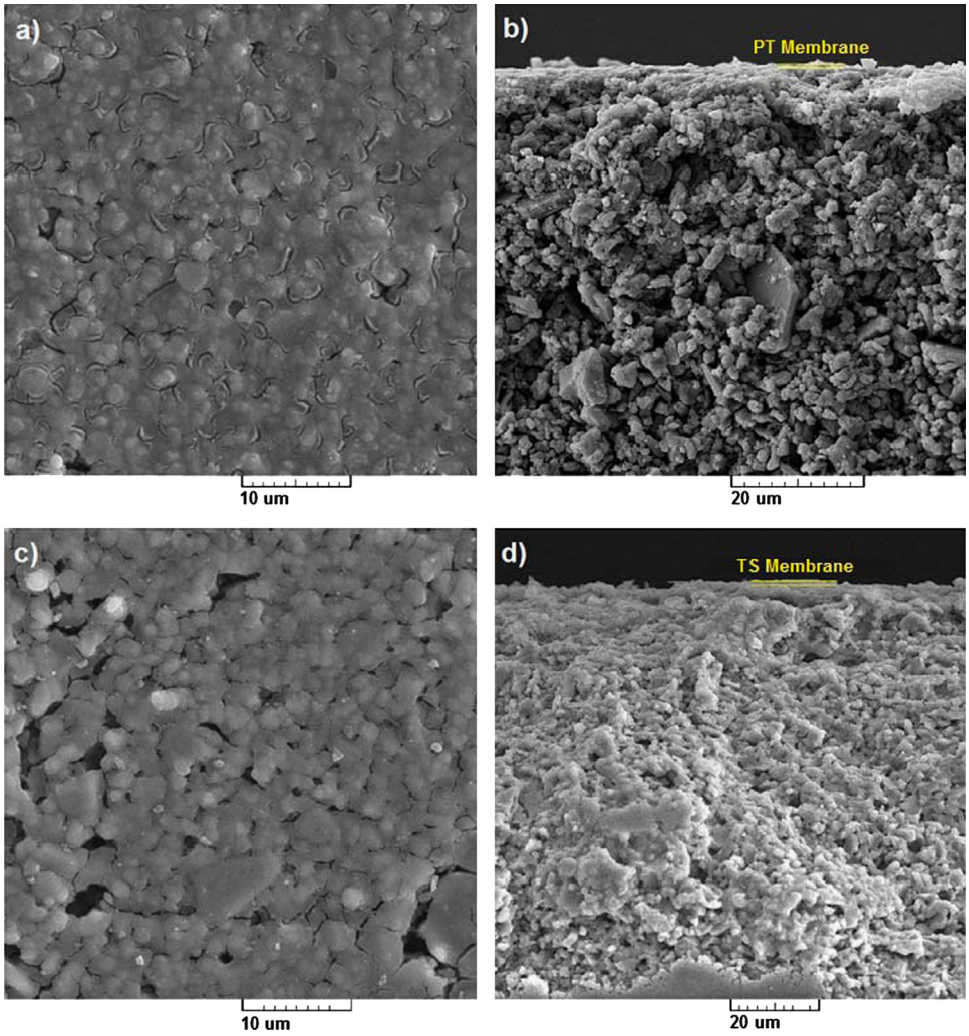

Fig. 8. FESEM micrographs of the surface and the cross–section of the (a and b) PT and (c and d) TS membranes.

about 10 nm that is in agreement with XRD results. Based on TEM image, the amorphous silica dopant in TiO_2 matrix could not be distinguished at this magnification. On the basis of our knowledge, the distinction of amorphous silica dopant in crystalline TiO_2 matrix (low silica content) is not reported.

3.2.1.3. AFM. Fig. 10 shows AFM micrographs of the surface morphology of the PT and TS membranes.

As revealed by AFM micrographs, the top layers of both membranes show pores in the range of 20–200 nm that are categorized in UF membranes group according to IUPAC. Also, from the AFM images it is seen that the TS membrane consists of smaller particles compared to the PT membrane. Also, the surface plot reveals that roughness of the TS membrane is clearly more than that of the PT membrane. The higher surface roughness allows a good ability to absorb photons for photocatalytic activity [9]. In fact, such a surface not only enables the adsorption of a greater number of pollutant molecules but also creates a rough environment where multiple light reflection occurs, thus considerably increasing the amount of absorbed photons [7].

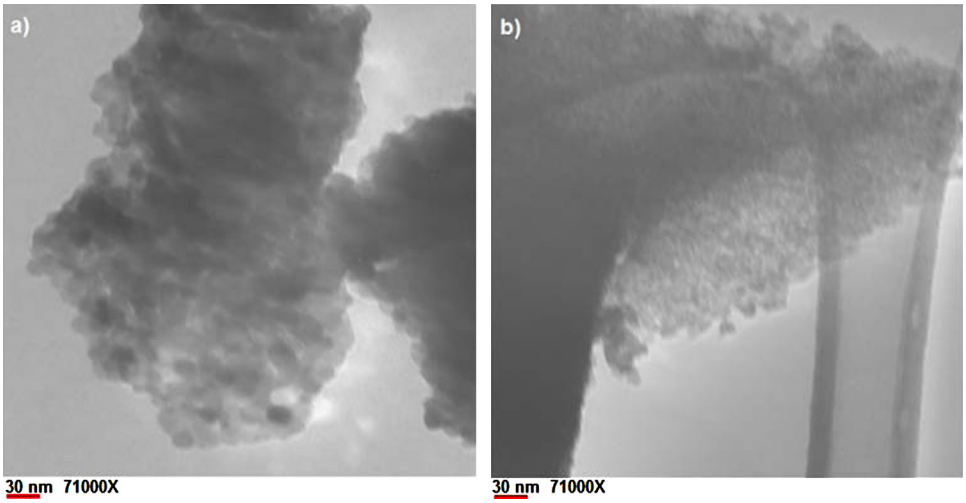

Fig. 9. TEM micrographs of the unsupported (a) PT and (b) TS membranes.

3.2.2. Photocatalytic properties

Photocatalytic activity of the PT and TS mesoporous membranes was determined by the absorbance change of MO feed solution under UV radiation after 60 min as shown in Fig. 11.

\By using Eq. (1), the MO removal efficiency of the PT and TS membranes was determined to be 21% and 63%, respectively.

It is well known that the photocatalytic activity of titania is greatly influenced by its crystal structure, grain size, surface area and surface hydroxyl content [15,16]. When silica is introduced to titania membrane, the prepared composite membrane may be different from titania membrane in both physical and chemical characteristics. These changes influence on the photocatalytic activity of the TS composite membrane compared to PT membrane. The results show that the photocatalytic activity of the TS membrane is more than that of the PT membrane. The increased photocatalytic activity can be attributed to the following factors. Firstly, when silica is added to the titania membrane, the grain size of titania drastically decreases (from 23.8 to 9.6 nm) and specific surface area obviously increases (from 32.8 to 99.14 m^2/g). The decrease in the crystallite size probably results in a larger driving force for charge transfer existing in a quantum-sized titania in the composite membrane. The increasing of surface area probably causes a higher adsorption toward organic contaminants. Also, the increase in surface hydroxyl content traps more holes in the valence band and thus prevents electron–hole recombination [42]. These factors enhance the photocatalytic activity of TS composite membranes. Therefore, though the TS composite membrane contains an amount of silica (which is a kind of insulator and has no photocatalytic activity), the photocatalytic activity of the composite membrane is still higher than that of the PT membrane. It can be concluded that a small amount of silica in the TS composite membrane plays a significant role in increasing photocatalytic activity.

Also, it seems that the higher roughness of the TS membrane (according to the AFM results in Fig. 10) allows a better ability to capture the incident photon energy since a larger surface extension facilitates the photo-degradation process. In fact, this surface not only enables the adsorption of a greater number of pollutant molecules but also creates a rough environment that causes a multiple light reflection and thus increases the amount of absorbed photons for photo-degradation process [9].

3.2.3. Permeation experiments

Separation performance of the nanostructured PT and TS membranes was evaluated via direct measurement of MO concentration in the permeate solution under 5 bar pressure. MO absorbance curves of the feed and the permeate solutions are depicted in Fig. 12.

MO concentration in the solutions was determined using calibration curve of MO (absorbance values of MO in 465 nm wavelength) as presented in Fig. 13.

The MO removal efficiency was determined to be 51% for the PT membrane and 60% for the TS membrane. The higher removal efficiency can be attributed to the smaller pores of the TS composite membrane according to BET analysis.

By coupling physical separation process with photocatalytic technique, the MO removal efficiency was remarkably improved up to 94%, while it was 63% and 60% with individual photocatalysis and separation techniques, respectively. Fig. 14 compares MO removal efficiency of the PT and TS mesoporous membranes obtained by the different techniques.

As observed, the TS mesoporous membrane synthesized in this work showed a high potential due to its multifunctional capability consisting of photo-degradiation and physical separation in water purification processes.

3.2.4. Water permeability

Water permeability of the nanostructured TP and TS membranes was compared by calculation of permeation flux under 5 bar pressure using Eq. (2). Based on the results, permeation flux was determined to be 9.35 L/m^2h for the PT membrane and 8.37 L/m^2h for the TS composite membrane.

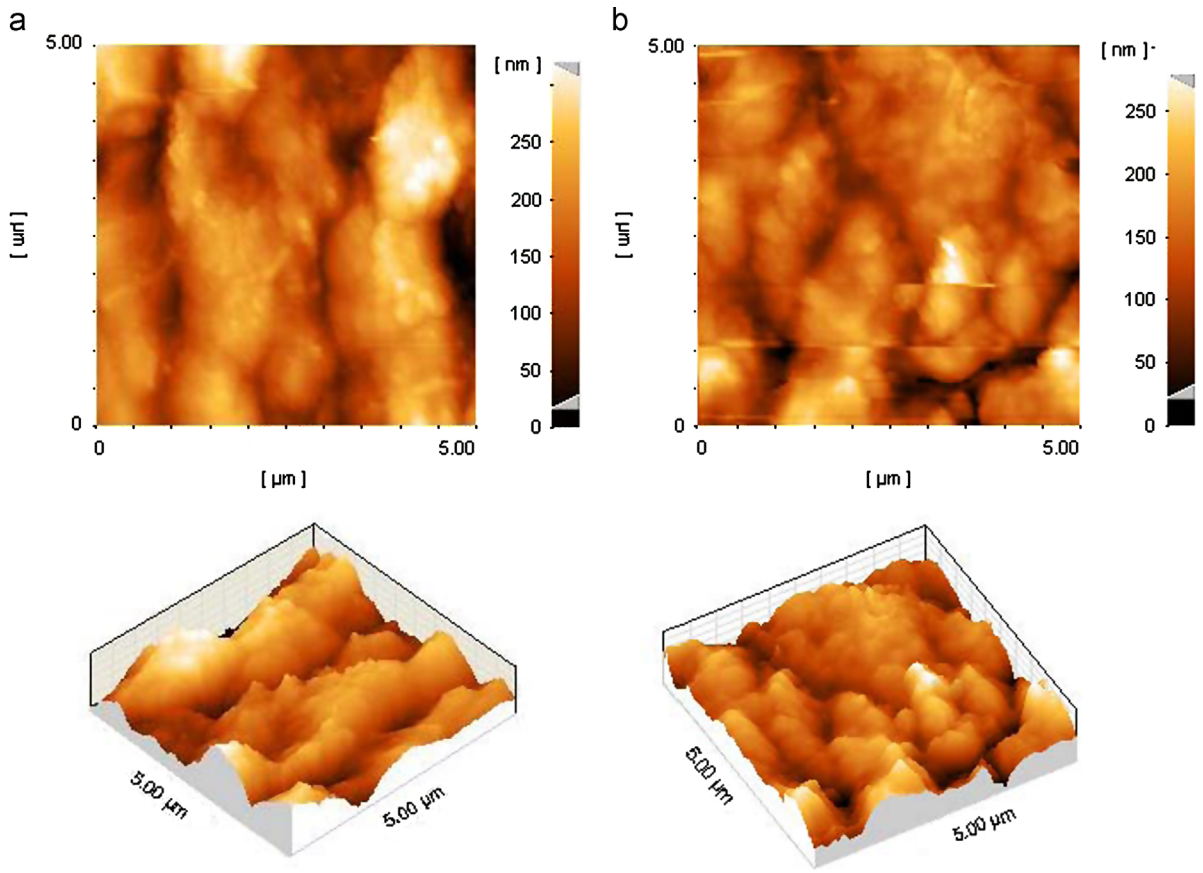

Fig. 10. AFM micrographs of the surface morphology of the (a) PT and (b) TS membranes.

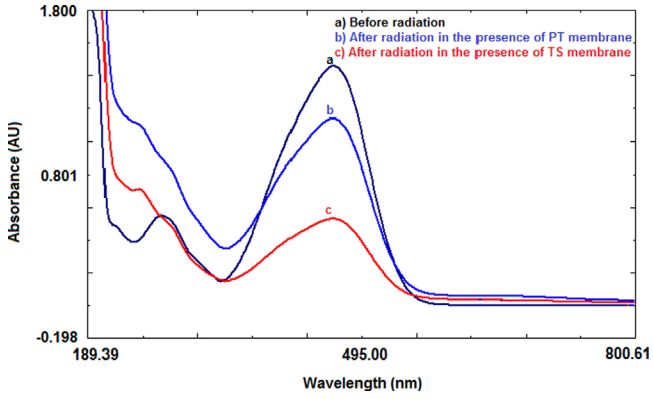

Fig. 11. Absorbance curves of MO aqueous solution in the presence of the PT and TS membrane before and after UV-radiation.

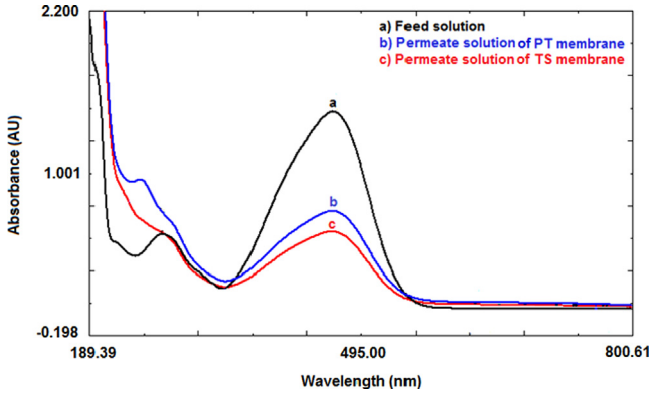

Fig. 12. MO absorbance curves of the feed and the permeate solutions.

This reduction can be attributed to the smaller pore size and the higher thickness of the TS membrane. Also, the permeate of PT and TS membranes was determined to be 103.8 and 92.9 mol $bar^{-1}m^{-2}h^{-1}$, respectively.

4. Conclusion

The nanostructured titania–silica membrane containing 5% silica was prepared by sol–gel method with simultaneous photocatalytic and physical separation capabilities for water purification. On the basis of results, silica addition to the titania membrane delays the phase transformation from anatase to rutile and inhibits grain growth of anatase. The resulting composite membrane was detected mesoporous, with the mean pore size of 3.94 nm, the crystallite size of 9.6 nm and the maximum BET surface area of 99.14 m^2/g. The removal efficiency of methyl orange using the pure titania membrane was determined to be 21% that increased up to 63% using the titania–silica membrane after 60 min UV-irradiation. The methyl orange separation performance was determined to be 51% for the pure titania membrane and up to 60% for the titania–silica composite membrane. By coupling membrane separation process with photocatalytic technique, the methyl orange removal efficiency of the titania–silica composite membrane was

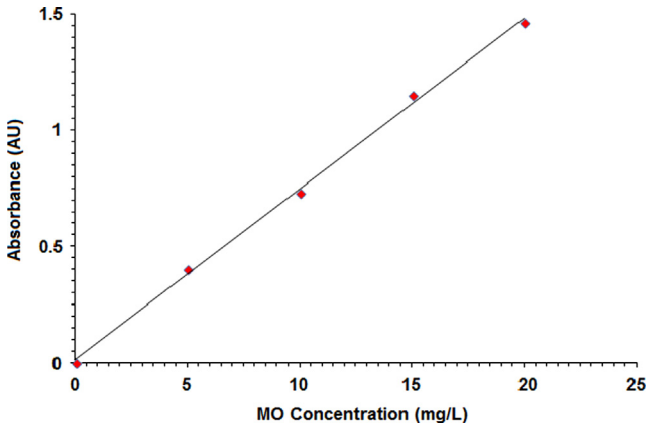

Fig. 13. Calibration curve of MO in 465 nm wavelength.

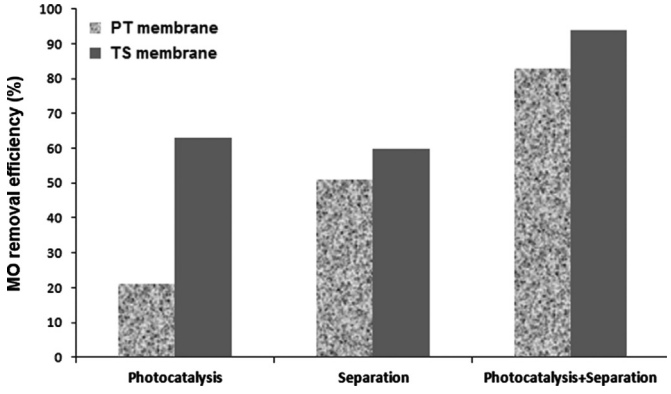

Fig. 14. MO removal efficiency of the PT and TS mesoporous membranes by the different techniques.

improved up to 94%. In present research, the synthesized titania–silica membrane showed a great potential in developing high efficient water treatment due to its multifunctional capability such as photo-degradation and physical separation.

Acknowledgment

The authors would like to thank Mr. I. Mozaffari for design and manufacturing of the photocatalytic membrane setup with a dead-end filtration cell used for filtration experiments.

References

[1] A.A. Habibpanah, S. Pourhashem, H. Sarpoolaky, Preparation and characterization of photocatalytic titania–alumina composite membranes by sol–gel methods, Journal of the European Ceramic Society 31 (2011) 2867–2875.

[2] A. Alem, H. Sarpoolaky, M. Keshmiri, Sol–gel preparation of titania multilayer membrane for photocatalytic applications, Ceramics International 35 (2009) 1837–1843.

[3] R.W. Baker, Membrane Technology and Applications, 2nd Ed., John Willey & Sons, California, 2000.

[4] H. Zhang, X. Quan, Sh. Chen, H. Zhao, Y. Zhao, Fabrication of photocatalytic membrane and evaluation its efficiency in removal of organic pollutants from water, Separation and Purification Technology 50 (2006) 147–155.

[5] H. Zhou, D.W. Smith, Advanced technologies in water and wastewater treatment, Journal of Environmental Science and Engineering 1 (2002) 247–264.

[6] C.P. Athanasekou, G.E. Romanos, F.K. Katsaros, K. Kordatos, V. Likodimos, P. Falaras, Very efficient composite titania membranes in hybrid ultrafiltration/photocatalysis water treatment processes, Journal of Membrane Science 392–393 (2012) 192–203.

[7] I.M. Arabatzis, S. Antonaraki, T. Stergiopoulos, A. Hiskia, E. Papaconstantinou, M.C Bernard, P. Falaras, Preparation, characterization and photocatalytic activity of nanocrystalline thin film TiO_2 catalysts towards 3,5-dichlorophenol degradation, Journal of Photochemistry and Photobiology A 149 (2002) 237.

[8] M.P. Reddy, A. Venugopal, M. Subrahmanyam, Hydroxyapatite photocatalytic degradation of calmagite (an azo dye) in aqueous suspension, Applied Catalysis B 69 (2007) 164–170.

[9] V. Tajer-Kajinebaf, H. Sarpoolaky, T. Mohammadi, Synthesis of nanostructured anatase mesoporous membranes with photocatalytic and separation capabilities for water ultrafiltration process, International Journal of Photoenergy (2013)http://dx.doi.org/10.1155/2013/509023.

[10] P. Cui, X. Zhao, M. Zhou, L. Wang, Photocatalysis–membrane separation coupling reactor and its application, Chinese Journal of Catalysis 27 (9) (2006) 752–754.

[11] R. Molinari, L. Palmisano, E. Drioli, M. Schiavello, Studies on various reactor configurations for coupling photocatalysis and membrane processes in water purification, Journal of Membrane Science 206 (2002) 399–415.

[12] S.H. Hyun, B.S. Kang, Synthesis of titania composite membranes by the pressurized sol–gel technique, Journal of the American Ceramic Society 79 (1) (1996) 279–282.

[13] H. Choi, E. Stathatos, D.D. Dionysiou, Photocatalytic TiO_2 films and membranes for the development of efficient wastewater treatment and reuse systems, Desalination 202 (2007) 199–206.

[14] S. Tursiloadi, H. Imai, H. Hirashima, Preparation and characterization of mesoporous titania–alumina ceramic by modified sol–gel method, Journal of Non-Crystalline Solids 350 (2004) 271–276.

[15] L. Sikong, J. Damchan, K. Kooptarnond, S. Niyomwas, Effect of doped SiO_2 and calcinations temperature on phase transformation of TiO_2 photocatalyst prepared by sol–gel method, Songklanakarin Journal of Science and Technology 30 (3) (2008) 385–391.

[16] K.G.K. Warrier, S. Rajesh Kumar, C.P. Sibu, High temperature stabilisation of pores in sol–gel titania in presence of silica, Journal of Porous Materials 8 (2001) 311–317.

[17] A.L. Castro, M.R. Nunes, A.P. Carvalho, F.M. Costa, M.H. Florêncio, Synthesis of anatase TiO_2 nanoparticles with high temperature stability and photocatalytic activity, Solid State Sciences 10 (2008) 602–606.

[18] Ch.He, B. Tan, J. Zhang, Thermally stable SiO_2-doped mesoporous anatase TiO_2 with large surface area and excellent photocatalytic activity, Journal of Colloid and Interface Science 344 (2010) 382–389.

[19] M.S.P. Francisco, V.R. Mastelaro, Inhibition of the anatase-rutile phase transformation with addition of CeO_2 to CuO–TiO_2 system: raman spectroscopy, X-ray diffraction, and textural studies, Chemistry of Materials, 14, 2514–2518.

[20] S. Vargas, R. Arroyo, E. Haro, R. Rodrıguez, Effects of cationic dopants on the phase transition temperature of titania prepared by the sol–gel method, Journal of Materials Research 14 (10) (1999) 3932–3937.

[21] G. Calleja, D.P. Serrano, R. Sanz, P. Pizarro, Mesostructured SiO_2-doped TiO_2 with enhanced thermal stability prepared by a soft-templating sol–gel route, Microporous and Mesoporous Materials 111 (2008) 429–440.

[22] P. Cheng, M. Zheng, Y. Jin, Q. Huang, M. Gu, Preparation and characterization of silica-doped titania photocatalyst through sol–gel method, Materials Letters 57 (2003) 2989–2994.

[23] C. Anderson, A.J. Bard, Improved photocatalytic activity and characterization of mixed TiO_2/SiO_2 and TiO_2/Al_2O_3 materials, Journal of Physical Chemistry B 101 (14) (1997) 2611–2616.

[24] J. Yu, J.C. Yu, The effect of SiO_2 addition on the grain size and photocatalytic activity of TiO_2 thin films, Journal of Sol–Gel Science and Technology 24 (2002) 95–103.

[25] C. Anderson, A.J. Bard, An improved photocatalyst of TiO_2/SiO_2 prepared by a sol–gel synthesis, Journal of Physical Chemistry 99 (1995) 9882–9885.

[26] S. Qourzal, N. Barka, M. Tamimi, A. Assabbane, A. Nounah, A. Ihlal, Y. Ait-Ichou, Sol–gel synthesis of TiO_2–SiO_2 photocatalyst for β-naphthol photodegradation, Materials Science and Engineering: C 29 (5) (2009) 1616–1620.
[27] A.A. Ismail, I.A. Ibrahim, M.S. Ahmed, R.M. Mohamed, H. El-Shall, Sol–gel synthesis of titania–silica photocatalyst for cyanide photodegradation, Journal of Photochemistry and Photobiology A 163 (2004) 445–451.
[28] M. Sivakumar, D.R. Mohan, R. Rangarajan, Studies on cellulose acetate-polysulfone ultrafiltration membranes: II. Effect of additive concentration, Journal of Membrane Science, 268, 208–219.
[29] E. Saljoughi, M. Sadrzadeh, T. Mohammadi, Effect of preparation variables on morphology and pure water permeation flux through asymmetric cellulose acetate membranes, Journal of Membrane Science 326 (2009) 627–634.
[30] S. Rajesh Kumar, C. Suresh, A.K. Vasudevan, N.R. Suja, P. Mukundan, K.G.K. Warrier, Phase transformation in sol–gel titania containing silica, Materials Letters 38 (1999) 161–166.
[31] P. Periyat, K.V. Baiju, P. Mukundan, P.K. Pillai, K.G.K. Warrier, High temperature stable mesoporous anatase TiO_2 photocatalyst achieved by silica addition, Applied Catalysis A 349 (2008) 13–19.
[32] Zh.Li, B. Hou, Y. Xu, D. Wu, Y. Sun, W. Hu, F. Deng, Comparative study of sol–gel-hydrothermal and sol–gel synthesis of titania–silica composite nanoparticles, Journal of Solid State Chemistry 178 (2005) 1395–1405.
[33] H. Zhang, X. Quan, Sh. Chen, H. Zhao, Fabrication and characterization of silica/titania nanotubes composite membrane with photocatalytic capability, Environmental Science and Technology 40 (2006) 6104–6109.
[34] C.P. Sibu, S.R. Kumar, P. Mukundan, K.G.K. Warrier, Structural modifications and associated properties of lanthanide oxide doped sol–gel nanosized titanium oxide, Chemistry of Materials 14 (2002) 2876–2881.
[35] F. Bosc, A. Ayral, P.A. Albouy, C. Guizard, A simple route for low-temperature synthesis of mesoporous and nanocrystalline anatase thin films, Chemistry of Materials 15 (12)) (2003) 2463–2468.
[36] A. Alem, H. Sarpoolaky, M. Keshmiri, Titania ultrafiltrationmembrane: preparation, characterization and photocatalytic activity, Journal of the European Ceramic Society 29 (4) (2009) 629–635.
[37] C.F. Song, M.K. Lu, P. Yang, D. Xu, D.R. Yuan, Structure and photoluminescence properties of sol–gel TiO_2–SiO_2 films, Thin Solid Films 413 (2002) 155–159.
[38] K.D. Kim, H.J. Bae, H.T. Kim, Synthesis and characterization of titania-coated silica fine particles by semi-batch process, Colloids and Surfaces A 224 (2003) 119–126.
[39] M. Jung, Synthesis and structural analysis of Au-doped TiO_2/SiO_2 mixed oxide films prepared by sol–gel process, Journal of Sol–Gel Science and Technology 19 (2000) 563–568.
[40] A.M. Seco, M.C. Goncalves, RM. Almeida, Densification of hybrid silica–titania sol–gel films studied by ellipsometry and FTIR, Materials Science and Engineering: B 76 (2000) 193–199.
[41] N. Yao, Sh. Cao, K.L. Yeung, Mesoporous TiO_2–SiO_2 aerogels with hierarchal pore structures, Microporous and Mesoporous Materials 117 (2009) 570–579.
[42] J.G. Yu, X.J. Zhao, Q.N. Zhao, Preparation, microstructure and photocatalytic activity of the porous TiO_2 anatase coating by sol–gel processing, Journal of Sol–Gel Science and Technology 7 (2) (2000) 163–171.